Regular Article

TRANSPLANTATION

Initiation of acute graft-versus-host disease by angiogenesis

Katarina Riesner,[1] Yu Shi,[1] Angela Jacobi,[2] Martin Kräter,[3] Martina Kalupa,[1] Aleixandria McGearey,[1] Sarah Mertlitz,[1] Steffen Cordes,[1] Jens-Florian Schrezenmeier,[1,4] Jörg Mengwasser,[1] Sabine Westphal,[1] Daniel Perez-Hernandez,[4] Clemens Schmitt,[1,4] Gunnar Dittmar,[4] Jochen Guck,[2] and Olaf Penack[1]

[1]Department of Hematology, Oncology and Tumor Immunology, Charité University Medicine, Campus Virchow Clinic, Berlin, Germany; [2]Biotechnology Center, and [3]University Clinic Carl Gustav Carus Dresden, Medical Clinic and Polyclinic 1, Technical University Dresden, Dresden, Germany; and [4]Max Delbrück Center for Molecular Medicine in the Helmholtz Association, Berlin, Germany

Key Points

- Angiogenesis preceded infiltration of inflammatory leukocytes during GVHD as well as during experimental colitis.
- Metabolic alterations and cytoskeleton changes occurred during early angiogenesis, but classical endothelial activation signs were absent.

The inhibition of inflammation-associated angiogenesis ameliorates inflammatory diseases by reducing the recruitment of tissue-infiltrating leukocytes. However, it is not known if angiogenesis has an active role during the initiation of inflammation or if it is merely a secondary effect occurring in response to stimuli by tissue-infiltrating leukocytes. Here, we show that angiogenesis precedes leukocyte infiltration in experimental models of inflammatory bowel disease and acute graft-versus-host disease (GVHD). We found that angiogenesis occurred as early as day+2 after allogeneic transplantation mainly in GVHD typical target organs skin, liver, and intestines, whereas no angiogenic changes appeared due to conditioning or syngeneic transplantation. The initiation phase of angiogenesis was not associated with classical endothelial cell (EC) activation signs, such as *Vegfa/VEGFR1+2* upregulation or increased adhesion molecule expression. During early GVHD at day+2, we found significant metabolic and cytoskeleton changes in target organ ECs in gene array and proteomic analyses. These modifications have significant functional consequences as indicated by profoundly higher deformation in real-time deformability cytometry. Our results demonstrate that metabolic changes trigger alterations in cell mechanics, leading to enhanced migratory and proliferative potential of ECs during the initiation of inflammation. Our study adds evidence to the hypothesis that angiogenesis is involved in the initiation of tissue inflammation during GVHD. (*Blood*. 2017;129(14):2021-2032)

Introduction

The number of allogeneic hematopoietic stem cell transplantations (bone marrow transplantations, allo-BMT) performed worldwide is increasing, as it often is the only curative treatment of hematologic malignancies. Despite the maximum use of therapeutic options, many patients die of acute graft-versus-host disease (GVHD), a systemic inflammatory disease primarily attacking liver, skin, and intestines, implicating a large unmet medical need for the development of novel therapies. There is increasing evidence demonstrating that the vascular endothelium can be used as a therapeutic target during GVHD.[1,2] In preclinical models as well as in patients, it has been demonstrated that GVHD is associated with the formation of new blood vessels.[2-5]

Under pathological conditions,[6-10] such as increased secretion of proangiogenic mediators by inflammatory cells, tissue damage, or oxygen and nutrient deficiency, endothelial cells (ECs) can rapidly form new blood vessels in a tightly orchestrated process. It involves the activation of ECs, the degradation of the extracellular matrix, the vessel sprouting relying on migratory, guiding "tip" cells and

elongating, proliferative "stalk" cells, morphogenesis, and the vessel stabilization by recruitment of pericytes. More recently, metabolic processes in ECs[11-13] involving fatty acid oxidation (FAO)[14,15] and glycolysis[16,17] have been shown to be important for initial steps of angiogenesis. Many of these processes can modulate angiogenic as well as inflammatory regulatory mechanisms and activating or targeting one can induce or modify the other,[7,8] underlining the importance of the crosstalk between angiogenesis and inflammation. In animal models of inflammatory diseases, such as inflammatory bowel disease (IBD) and GVHD, it has been demonstrated that the inhibition of angiogenesis can be used therapeutically to reduce the recruitment of tissue-infiltrating leukocytes.[4,8,18,19] However, it is not known if angiogenesis contributes to the initiation of inflammation or is a mere consequence of inflammation.[20]

We analyzed the role of angiogenesis during the initiation of inflammation in experimental models of IBD and GVHD, which occurs after allogeneic hematopoietic stem cell transplantation.

There is an Inside *Blood* Commentary on this article in this issue.

Materials and methods

Study design and statistics

Sample size for GVHD experiments was calculated by estimation of time point–specific analyses based on the Student t test assuming–80% power and 0.05 2-sided level of significance. Experiments with at least 5 animals per group (untreated [naïve], conditioned-only [chemo], allogeneic [ALLO], or syngeneic [SYN] transplanted mice) were performed 2 times.

Specific time points for analyses were chosen after initial time course experiment. All collected data were used in statistical analyses, only excluding animals that died before specific time points for data collection. Animals were randomized, including equal distribution of weight status and mixed housing of different transplanted animals. For subsequent analyses, transplant conditions were encoded. All experiments were approved by the Regional Ethics Committee for Animal Research (State Office of Health and Social Affairs, Berlin).

Survival data were analyzed using the Kaplan-Meier method and compared with the Mantel-Cox log-rank test. For all other data, the Student unpaired t test (2-tailed) was used if not indicated differently. Normality tests and F test confirmed Gaussian distribution and equality of variance between different groups. Values are presented as mean $\pm$ standard error of the mean (SEM). Values of $P \leq .05$ were considered statistically significant. All statistical analyses were performed using GraphPad Prism software (GraphPad Software Inc, La Jolla, CA).

Mice

Female C57BL/6 (B6) (H2^b), 129S2/SvPasCrl (129) (H2^b), LP/J (H2^b), B6D2F1 (BDF) (H2$^{b/d}$), BALB/c (H2^d), B6.Cg-Tg(CAG-DsRed*MST)1Nagy/J (DsRed+B6) (H2^b) mice (10–12 weeks old) were purchased from Charles River Laboratories (Sulzfeld, Germany) and housed in the Charité University Hospital Animal Facility. Mice were individually scored twice a week for 5 clinical parameters (posture, activity, fur, skin, and weight loss) on a scale from 0 to 2. Clinical GVHD score was assessed by summation of these parameters. Survival was monitored daily.

GVHD experiments

For GVHD models LP/J→B6, B6→BDF, 129S2/Sv→B6, DsRed+B6→BDF, recipient mice received intraperitoneal doses of 20 mg/kg per day busulfan (Sigma-Aldrich, St. Louis, MO) for 5 days, followed by 100 mg/kg per day cyclophosphamide (Sigma-Aldrich) for 3 days and were injected intravenously with 1.5×10^7 bone marrow (BM) cells and 2×10^6 splenic T cells from allogeneic and syngeneic donor mice on day 0. For B6→BALB/c, recipient mice received 900 cGy total body irradiation from a ^{137}Cs source as a split dose with a 3-hour interval and were injected intravenously with 5×10^5 BM cells and 1×10^6 splenic T cells. BM was flushed from the tibia and femur, and single-cell suspension was prepared in phosphate-buffered saline (PBS)/2% fetal calf serum/1 mm EDTA by gently passing through a 23-G needle and over a 70-μm cell strainer (BD Biosciences, San Jose, CA). Splenic T-cell suspension was obtained using the Pan T-cell Isolation Kit II (Miltenyi Biotec, Bergisch Gladbach, Germany). For vascular endothelial growth factor A (VEGFA) inhibition, LP/J→B6, B6 mice were treated intraperitoneally 2 times a week with 5 mg/kg B20-4.1.1 (Genentech, South San Francisco, CA) or 5 mg/kg rat immunoglobulin G2 (IgG2; Sigma-Aldrich). For VEGFR1/2 inhibition, B6→BALB/c, BALB/c mice were treated intraperitoneally on days 0, +2, +4, +8, +10 with a combination of 800 μg DC101 and MF1 (ImClone Systems, New York, NY) or with 800 μg rat IgG2.

Colitis (IBD) experiments

For colitis induction, 3% dextran sulfate sodium (DSS; MP Biomedicals, Santa Ana, CA) was administered to B6 mice in drinking water. For DsRed colitis experiments, B6 mice received 1.5×10^7 BM cells from DsRed+B6; at day+40 after BMT, DsRed+BM chimeras with >90% DsRed$^+$ cells in blood were used for DSS induction. For endothelial progenitor cell (EPC) experiments, B6 mice received on the day of DSS induction intravenously 5×10^4 DsRed+EPCs,

which were fluorescence-activated cell sorted (FACS) (CD11b$^-$, Ter119$^-$, c-Kit$^+$, VEGFR2$^+$) from DsRed+B6 BM using a Bio-Rad S3 Cell Sorter. Purity was 90% or higher.

Immune fluorescence staining

Tissue samples were cryoembedded in Tissue-Tek (Sakura Finetek, Alphen aan den Rijn, The Netherlands). Sections measuring 7 μm were acetone fixed (-20°C), blocked with PBS/3% bovine serum albumin /5% fetal calf serum, and stained overnight at 4°C with primary rat monoclonal antibodies (mAbs) against CD4 (H129.19, 1:500), CD8 (53-6.7, 1:500), CD11b (M1/70, 1:200), Gr1/Ly-6G (RB6-8C5, 1:200), major histocompatibility complex-I (MHC-I)/H2kb (AF6-88.5, 1:200), CD31 (MEC13.3, 1:400), panendothelial cell antigen (MECA-32, 1:500) from BD Biosciences and MHC-II (ER-TR3, 1:200) from BMA Biomedicals (Augst, Switzerland); with hamster mAb against CD31 (2H8, 1:500) and rabbit polyclonal Ab against Ki67 (PA5-19462, 1:200) from Thermo Fisher Scientific (Waltham, MA). For visualization, 1:1000 secondary donkey anti-rat antibody Alexa Fluor 488 and goat anti-rabbit antibody Alexa 555 (Life Technologies, Carlsbad, CA), goat anti-hamster Cy3 (Jackson ImmunoResearch, West Grove, PA), and nuclear counterstaining with 4',6-diamidino-2-phenylindole (Sigma-Aldrich) were used. To determine Marker$^+$ area, 6 sections per sample were investigated with the $\times 20/0.50$ objective of BA410 epifluorescence microscope (Motic, Causeway Bay, Hong Kong), and pictures were acquired with Moticam Pro 285B camera and Motic Images Plus 2.0 Software from Motic. Marker$^+$ area to total area was quantified with a predetermined threshold using Fiji Software (http://fiji.sc/Fiji). Increase in vascular density was determined by elevated percentage of positive area of the stained EC marker CD31 or MECA. For analysis of EC proliferation, 10 high-power-field photographs per sample were taken with the $\times 40/0.75$ objective of a BA410 epifluorescence microscope. The number of Ki-67$^+$ cells in direct contact with CD31 signal (Ki67$^+$ ECs) per high-power field was counted. For Z-stacks, 21-μm sections were analyzed with a Zeiss LSM700 microscope (Carl Zeiss AG, Oberkochen, Germany), and 20 sections per picture were taken.

Flow cytometry

Cells were washed twice and stained for 20 minutes at 4°C in PBS/0.5 mM EDTA/0.5% bovine serum albumin with the following rat mAbs from BD Biosciences: anti-CD31 (MEC13.3-APC and PE), anti-VEGFR2 (AVAS12α1-PE), anti-ICAM (3E2-PE), anti-ckit (2B8-APC), anti-CD45 (30F11-PerCP-Cy5.5 and FITC), anti-CD11b (M1/70-APC-Cy7), anti-Ter119 (Ter119-PE-Cy7), anti-H2kb (AF6-88.5-FITC). Samples were analyzed by BD FACSCanto II (BD Biosciences) and FlowJo 7.6.5 Software (TreeStar Inc, Ashland, OR). In liver, ECs were determined as Ter119-CD11b-CD45dim/$-$CD31$^+$ cells.

Quantitative real-time PCR

RNA and complementary DNA, obtained using the RNeasy Mini Kit (Qiagen, Venlo, The Netherlands) and the QuantiTect Reverse Transcription Kit (Qiagen) following the manufacturer's instructions, were amplified (50°C, 2 minutes; 95°C, 10 minutes; 49 cycles of 95°C, 10 seconds; 60°C, 1 minute) on DNA Engine Opticon (Bio-Rad, Hercules, CA) using the TaqMan Gene Expression Master Mix (Life Technologies), and *Vegfa*, *VEGFR2*, *Icam1*, *Vcam1*, *P-* and *E-selectin* primers and probe from BioTez GmbH (Berlin, Germany). Data were analyzed with Opticon Monitor 3.1 analysis software (Bio-Rad) and the comparative CT Method ($\Delta\Delta$CT Method).

EC isolation

Single-cell suspensions from liver and colon were generated via digestion at 37°C and continuous shaking with 2 mg/mL Collagenase D (Roche Diagnostics, Rotkreuz, Switzerland) for 45 minutes and 1 mg/mL collagenase IV (Sigma-Aldrich) for 60 minutes, respectively. Cells were passed twice over a 70-μm cell strainer. Liver ECs were additionally enriched with gradient centrifugation using 30% Histodenz (Sigma-Aldrich) according to manufacturer's instructions. For pure EC populations, liver cells were magnetic-activated cell sorted (MACS)–isolated using CD146 liver sinusoidal endothelial cells (LSEC) Microbeads (Miltenyi Biotec) after manufacturer's instructions, and colon cells were FACS-sorted (CD11b$^-$, CD45dim/$-$,
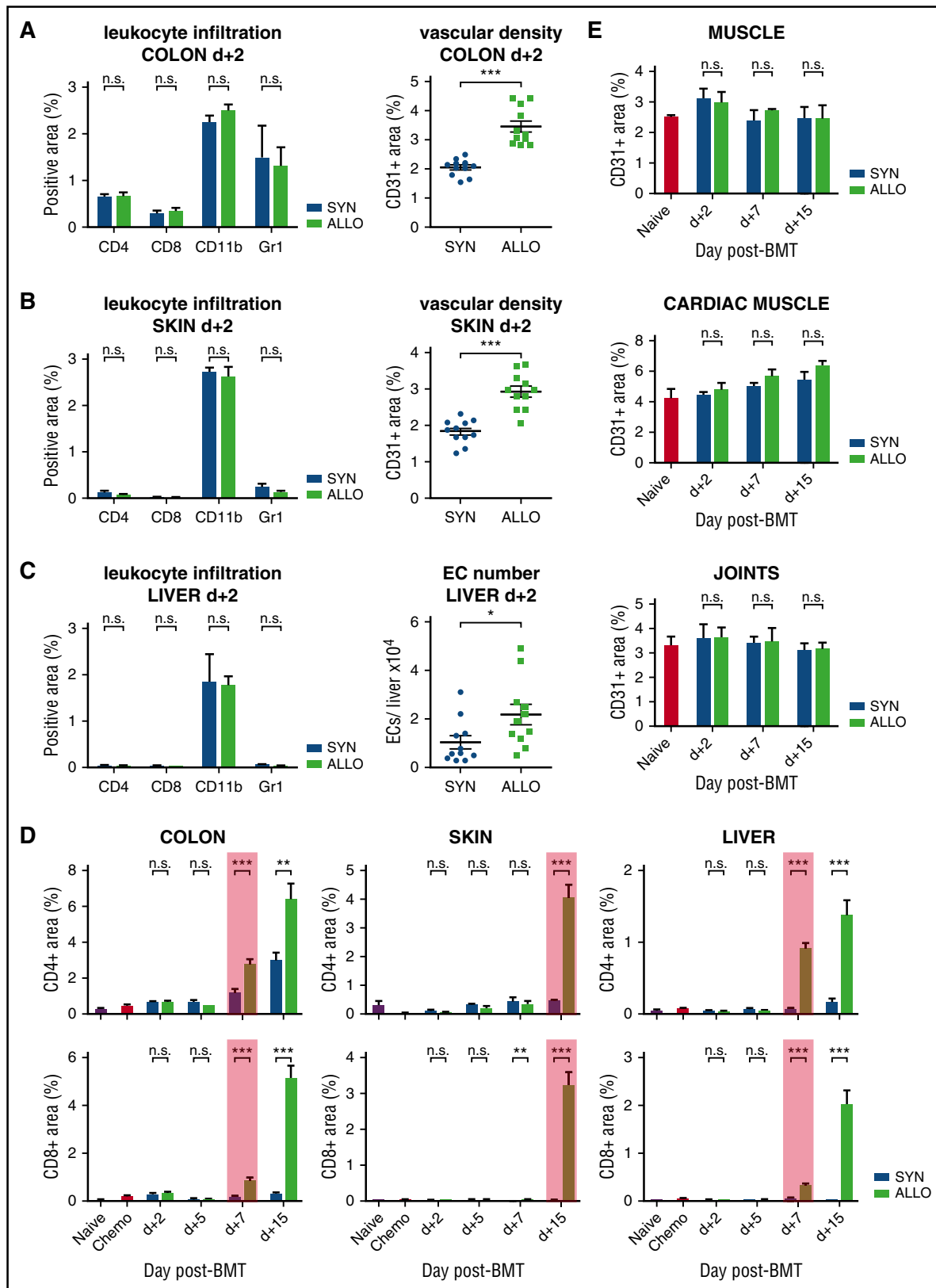
Figure 1. Angiogenesis occurs exclusively in target organs and precedes leukocyte infiltration during GHVD. (A-C) Leukocyte infiltration: percentage of CD4-, CD8-, CD11b-, and Gr1-positive area in GVHD-target organs colon, skin, and liver of allogeneic (ALLO) compared with syngeneic transplanted mice (SYN) 2 days (d+2) after BMT. Vascular density: percentage of CD31-positive area in colon and skin and EC number in liver of SYN and ALLO mice at day+2 after BMT. (D) Time course of CD4$^+$ and CD8$^+$ lymphocyte infiltration. The red box marks first significant increase in CD4- and CD8-positive area in ALLO mice. Untreated (Naive) and only chemotherapy-conditioned (Chemo) mice served as control and showed no infiltration. (E) Vascular density in nonclassical target organs skeletal and cardiac muscle and joints at day+2, +7, and +15 after BMT. Untreated mice (Naive) served as control. Data pooled from 2 independent experiments (naive, chemo, n = 5 per group; SYN, ALLO, n = 10-12 per group). Error bars indicate mean ± SEM. *$P < .05$; **$P < .01$; ***$P < .001$; n.s., not significant by Student t test (2-tailed).

CD31^{+}) using a Bio-Rad S3 cell sorter. Purity was checked via flow cytometry analysis of ICAM1 and CD31.

Microarray analysis

Total RNA from colon EC was isolated with the mirVana miRNA Isolation Kit (Life Technologies) and subjected to microarray analysis (GeneChip Mouse Gene 2.0 ST Array; Affymetrix). Obtained raw data were normalized with Expression Console Software and analyzed with Transcriptome Analysis Console Software (Affymetrix) with the following parameters: Fold Change (linear) < −2 or >2, analysis of variance P value (Condition pair) < 0.05.

LC-MS/MS proteome analysis

At day+2 after BMT, proteins from liver EC from allogeneic- and syngeneic-transplanted mice were isolated and quantified by dimethylation labeling,[21,22] subjected to high through-put liquid chromatography tandem-mass spectrometry (LC-MS/MS) analysis, and MS data were processed[23,24] as described in detail in the supplemental Material and methods, available on the *Blood* Web site. Quantitative ratios were calculated and normalized by Max Quant software package. R software (Version 3.0.0, www.r-project.org) was used to calculate log2 ratios between syn- and allo-transplanted groups, log10 of signal intensities, and P values of protein abundance changes. P values < .05 were chosen as statistically significant. Normalized ratios were used for differential expression analysis (up ≥1.3 or down ≤0.44). Protein information (names, cellular localization, involved functions, and pathways) were obtained from UniProtKB (http://www.uniprot.org/).

Real-time deformability cytometry

At day+2 after BMT, liver EC from allogeneic- and syngeneic-transplanted mice were isolated, and real-time deformability cytometry (RT-DC) measurements were performed as previously described.[25,26] For details on procedures, see the supplemental Material and Methods.

Results

Angiogenesis precedes lymphocyte infiltration in acute GVHD and in an experimental model of IBD

To shed light onto initial mechanisms of both processes after allo-BMT, we first determined the time course of angiogenesis (supplemental Figure 1) as well as of leukocyte infiltration in a clinically relevant murine MHC-matched, minor histocompatibility antigen–mismatched GVHD model (LP/J [H2kb] →C57BL/6 [H2kb]).[27] In allo-BMT recipients, we found significant increased vascular density in the colon and skin and significantly increased EC numbers in liver already on day+2 after BMT (Figure 1A-C). In contrast, infiltration of CD4^{+} and CD8^{+} T cells into GVHD target organs did not occur until day+7 in colon and liver and until day+15 in skin (Figure 1D). Also, the pan myeloid cell marker CD11b as well as the neutrophil marker Gr-1/Ly-6G did not show significant differences in the GVHD target organs at day+2, emphasizing that monocytes/macrophages/neutrophils as well as lymphocytes did not infiltrate prior to the occurrence of angiogenesis (Figure 1A-C). Strikingly, conditioned mice and syn-BMT recipients exhibited no change in vascular density, showing that early angiogenesis was specific to GVHD and allo-BMT (supplemental Figures 1 and 2A,B). We confirmed the results with another panendothelial cell marker MECA-32 (supplemental Figure 3) and in 2 other murine GVHD models (129S2/SvPasCrl→C57BL/6 and C57BL/6→B6D2F1) (supplemental Figures 4A,B and 5). Our results demonstrate that angiogenesis is an initial event during

GVHD, whereas GVHD-associated infiltration of inflammatory cells occurs secondarily.

We asked the question if initial angiogenesis is specific to GVHD or likewise precedes infiltration of leukocytes in other inflammatory diseases. In a standard model for IBD, the DSS-induced colitis (supplemental Figure 6A) was found to have similar results to GVHD experiments. CD31^{+} vascular density was significantly increased already at day+1 after colitis induction (supplemental Figure 6B-D), whereas infiltration of CD4^{+}, CD8^{+}, and CD11b^{+} cells was not significantly increased in colon until day+3 (supplemental Figure 6B, C,E-G).

GVHD non–target organs showed no angiogenesis and lymphocyte infiltration

To investigate if early angiogenesis occurs in the context of systemic inflammation or is specific to GVHD target organs, we analyzed joints, skeletal, and cardiac muscle. These organs are prone to angiogenesis under pathological conditions,[6,7,28] but they are typically not affected by acute GVHD. We found no significant change in vascular density as well as no lymphocyte infiltration in the non–classical target organs of allo-BMT vs syn-BMT recipients at day+2 or any later time points (Figures 1E; supplemental Figure 7).

No early incorporation of EPCs in experimental models of GVHD and IBD

Next, we analyzed if the early increase in vascular density is dependent on the proliferation of resident tissue ECs (angiogenesis) or on the incorporation of BM-derived EPCs, termed vasculogenesis.[8] We first confirmed that at day+2 after BMT, allo-BMT recipients showed increased numbers of proliferating (Ki67^{+}) ECs in colon compared with syn-BMT recipients (Figure 2A). To determine EPC incorporation, we transplanted B6D2F1 mice with DsRed+C57BL/6 BM cells and T cells to induce GVHD. We could not detect costaining signals of DsRed and CD31 in colon and skin of allo-BMT recipients at day+2 (Figure 2B). Similarly, DsRed[+] BM chimeras as well as C57BL/6 mice receiving EPCs from DsRed+C57BL/6 BM showed no significant amount of CD31+DsRed^{+} coexpressing cells in colon until day+4 after induction of colitis (Figure 2C,D). Our data suggest that the initial formation of blood vessels during GVHD and during experimental colitis is due to the formation of new blood vessels from existing ones, termed angiogenesis.

Effect of targeting angiogenesis in GVHD by blocking Vegfa/VEGFR pathway

We aimed at identifying pathways that are relevant for early angiogenesis during GVHD and initially investigated the *Vegfa/VEGFR1+2* axis.[29] Based on our previous observation demonstrating a reduction of GVHD due to inhibition of neovascularization by anti-VE-cadherin antibodies,[4] we performed therapeutic interventions with monoclonal blocking antibodies. The anti-*VEGFA* antibody B20-4.1.1 had no significant effects on survival and GVHD scores during GVHD (Figure 3A). *VEGFR1+2*-blocking by administration of MF1 and DC101 led to inhibition of hematopoietic reconstitution (supplemental Figure 8) and decreased survival after allo-BMT (Figure 3B). Furthermore, we found no consistent upregulation of *Vegfa* and *VEGFR2* expression levels in GVHD-target organs during the initiation of GVHD (Figure 3C,D) or later time points (Figure 3E). Taken together, our results argue against an important role of the *Vegfa/VEGFR2* pathway for initiation of angiogenesis in GVHD target organs.

Figure 2. No early incorporation of EPCs in experimental models of GVHD and IBD. (A) Number of proliferating (Ki67^{+}) ECs in colon of SYN and ALLO mice at day+2 after BMT (n = 3 per group). White arrow marks proliferating EC (4′,6-diamidino-2-phenylindole [DAPI[+]] [blue], Ki67^{+} [red-A555] in direct contact with CD31 [green-A488] signal). White asterisks mark proliferating crypt cells. (B) Representative pictures of green-A488 CD31 (vessel-related), DsRed (BM-related), and merged signals of colon and skin sections from SYN and ALLO mice at day+2 after BMT (DsRed+C57BL/6→B6D2F1). (C) Representative pictures of green-A488 CD31, DsRed, and merged signals of colon sections from DsRed[+] BM chimeras at day+4 after DSS colitis induction. (D) Representative projections of Z-stacks of colon samples at day+4 after DSS induction from colitis-bearing and control mice, which received DsRed[+] EPCs. Green A488-CD31 signal is vessel-related. Scale bar, 30 μm (A-C). Error bar indicates mean ± SEM. *P < .05 by Student t test (2-tailed).
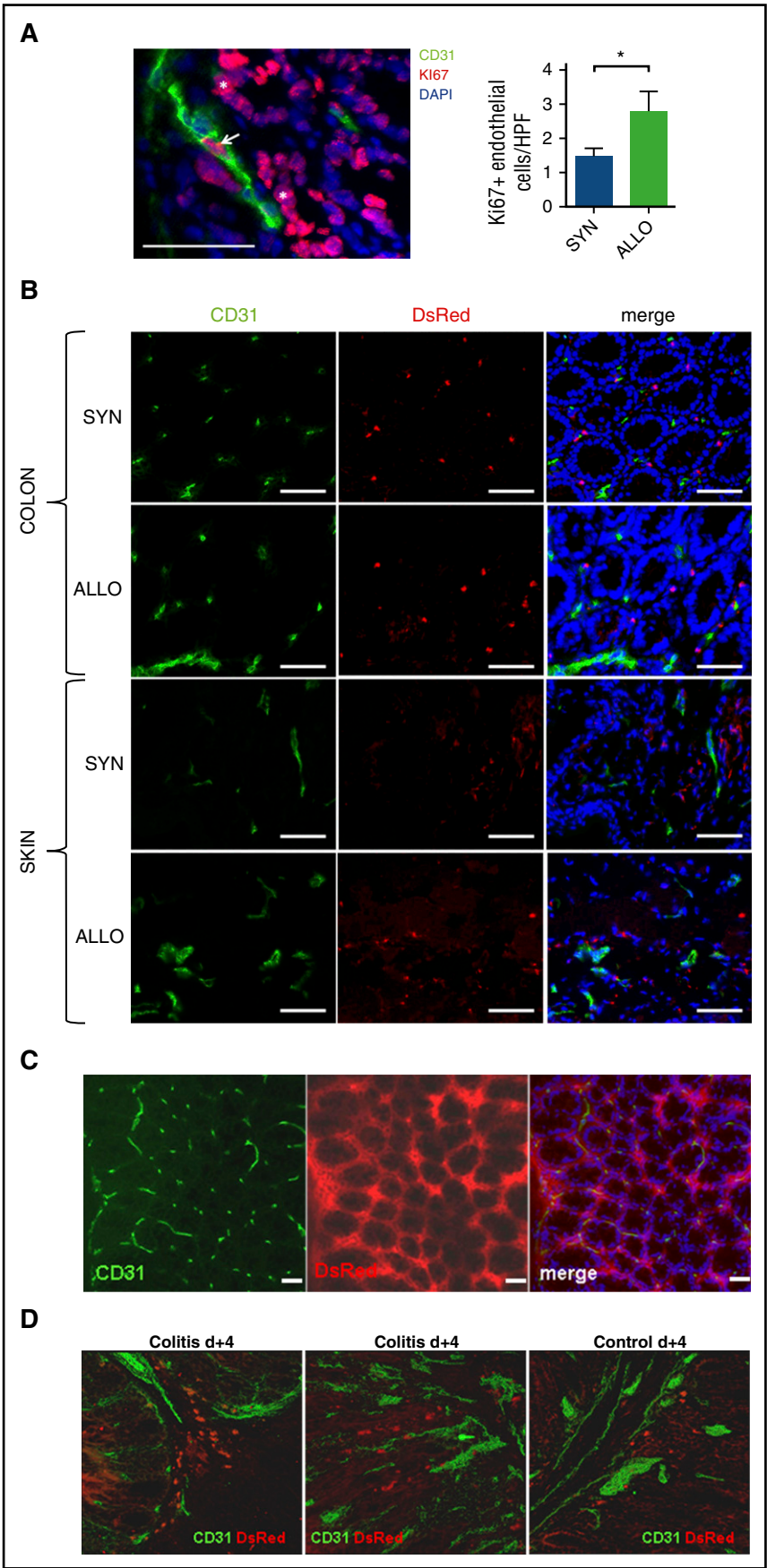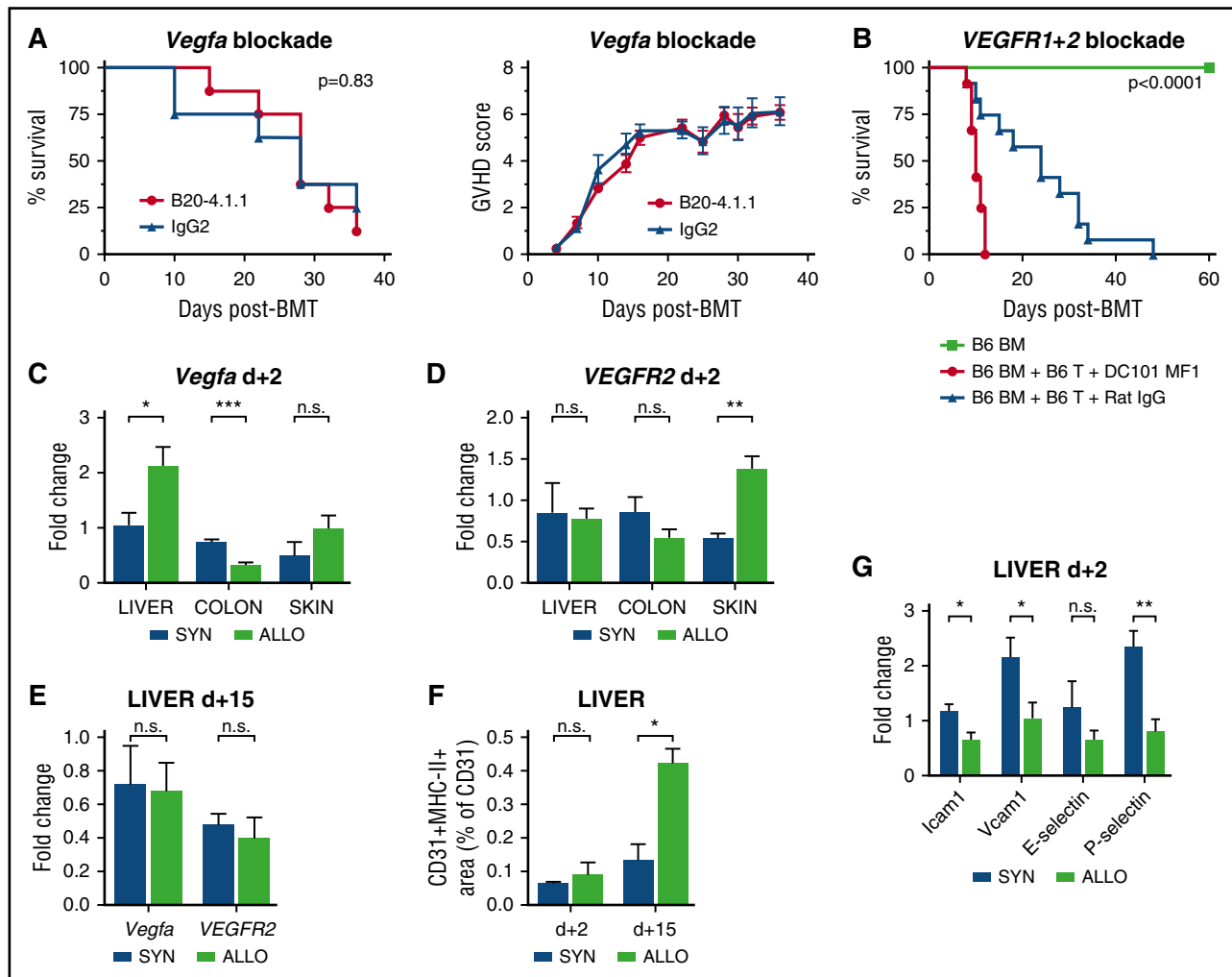
Figure 3. The *Vegfa/VEGFR2* pathway and adhesion molecules are not upregulated during the initiation of angiogenesis in GVHD target organs. (A) Kaplan-Meier curve and GVHD scoring of B20-4.1.1 (*Vegfa* inhibitor) and rat IgG2-treated control mice (LP/J→C57BL/6) (n = 8 per group). (B) Kaplan-Meier curve of DC101+MFI (*VEGFR1+2* inhibitor) and rat IgG–treated control mice (C57BL/6→BALB/c) (n = 12 per group). Untreated, only BM cell transplanted mice served as internal control (n = 5). *Vegfa* and *VEGFR2* expression in GVHD target organs liver, colon, and skin of ALLO vs SYN mice (n = 5 per group) at day+2 after BMT (C-D) as well as in liver at day+15 after BMT (E). (F) MHC-II and CD31 double-positive area of CD31-positive area in liver of SYN and ALLO mice day+2 and +15 after BMT (n = 7 per group). (G) Expression of adhesion molecules Intercellular Adhesion Molecule 1 (*Icam1*), vascular cell adhesion molecule 1 (*Vcam1*), *E-selectin*, and *P-selectin* in MACS-sorted liver ECs from SYN vs ALLO mice at day+2 after BMT (n = 5). In panels A-B, *P* values were calculated by using the log-rank test. In panels C-E,G, gene expression levels were normalized to *Gapdh* expression and are shown relative to gene levels of a reference untreated sample. Error bars indicate mean ± SEM. *P < .05; **P < .01; ***P < .001; n.s. not significant by Student *t* test (2-tailed).

Expression levels of inflammation-associated endothelial activation markers in GVHD

We next investigated EC activation and adhesion molecules during early and established GVHD. ECs constitutively express MHC-I,[30,31] which did not change after transplantation (supplemental Figure 9A,B). In a highly inflammatory environment at day+15, we found a significant increase in MHC-II+CD31$^+$ area in liver of allo-BMT recipients, whereas in a leukocyte infiltration-free environment at day+2, no MHC-II upregulation occurred (Figure 3F). Typical for inflammatory diseases, we found increased expression levels of adhesion molecules, such as *Icam1*, *Vcam1*, *E-*, and *P-selectin* in GVHD target organs (supplemental Figure 10) during established GVHD at day+15. In sharp contrast, at day+2 MACS-isolated CD45dim+neg/CD11b$^-$/CD31$^+$ liver ECs of allo-BMT recipients (supplemental Figure 11A,B) showed significant downregulation of gene expression levels of these markers compared with syn-BMT recipients (Figure 3G). Our results demonstrate that initial endothelial activation follows a different pattern as compared with endothelial activation during established GVHD.

Metabolic and cytoskeleton changes in ECs lead to higher deformability

To identify pathways during the initiation of angiogenesis in an unbiased approach, we performed microarray analyses of FACS-sorted colon ECs in allo-BMT recipients vs syn-BMT recipients at day+2. Hierarchical clustering revealed profound differences in gene expression in colon ECs during the initiation of GVHD in allo-BMT vs syn-BMT (Figure 4A, C). To detect relevant changes on protein level during the initiation of angiogenesis, we performed LC-MS/MS proteome analyses of MACS-isolated liver ECs at day+2 after allo-BMT vs syn-BMT. We identified 18 upregulated and 25 downregulated proteins (Figure 5A-C) showing network connections (supplemental Figures 12 and 13). A list of significant upregulated and downregulated genes and proteins is given in supplemental Tables 1-4. Again, no upregulation of *Vegfa* and *VEGFR2* was detected, and several adhesion molecules were downregulated, including *Icam1*, *Muc1*, CAMD3, SCARB2, and OSTF1. Strikingly, we detected substantial changes in the lipid and sphingolipid metabolism as well as in glycolysis of ECs during early GVHD in colon and liver on
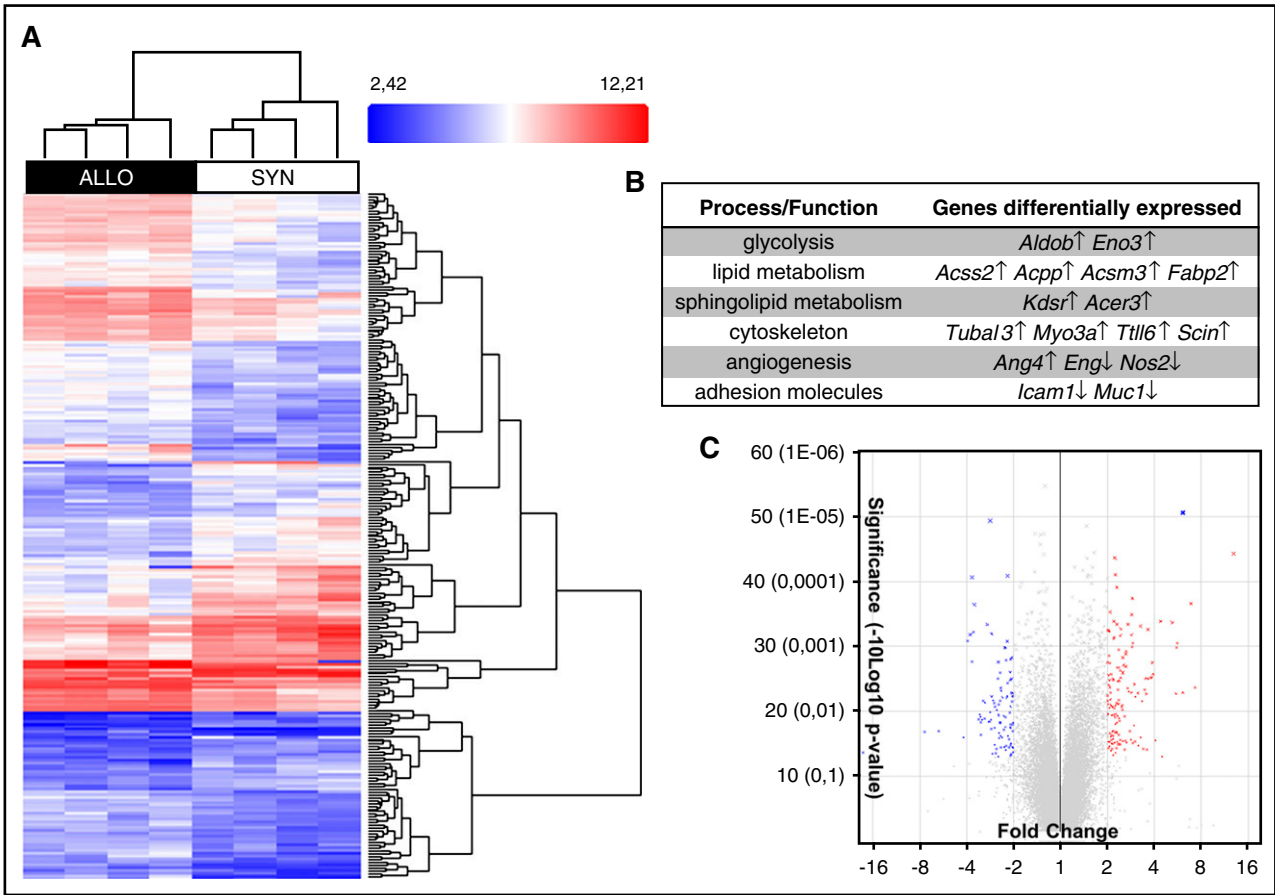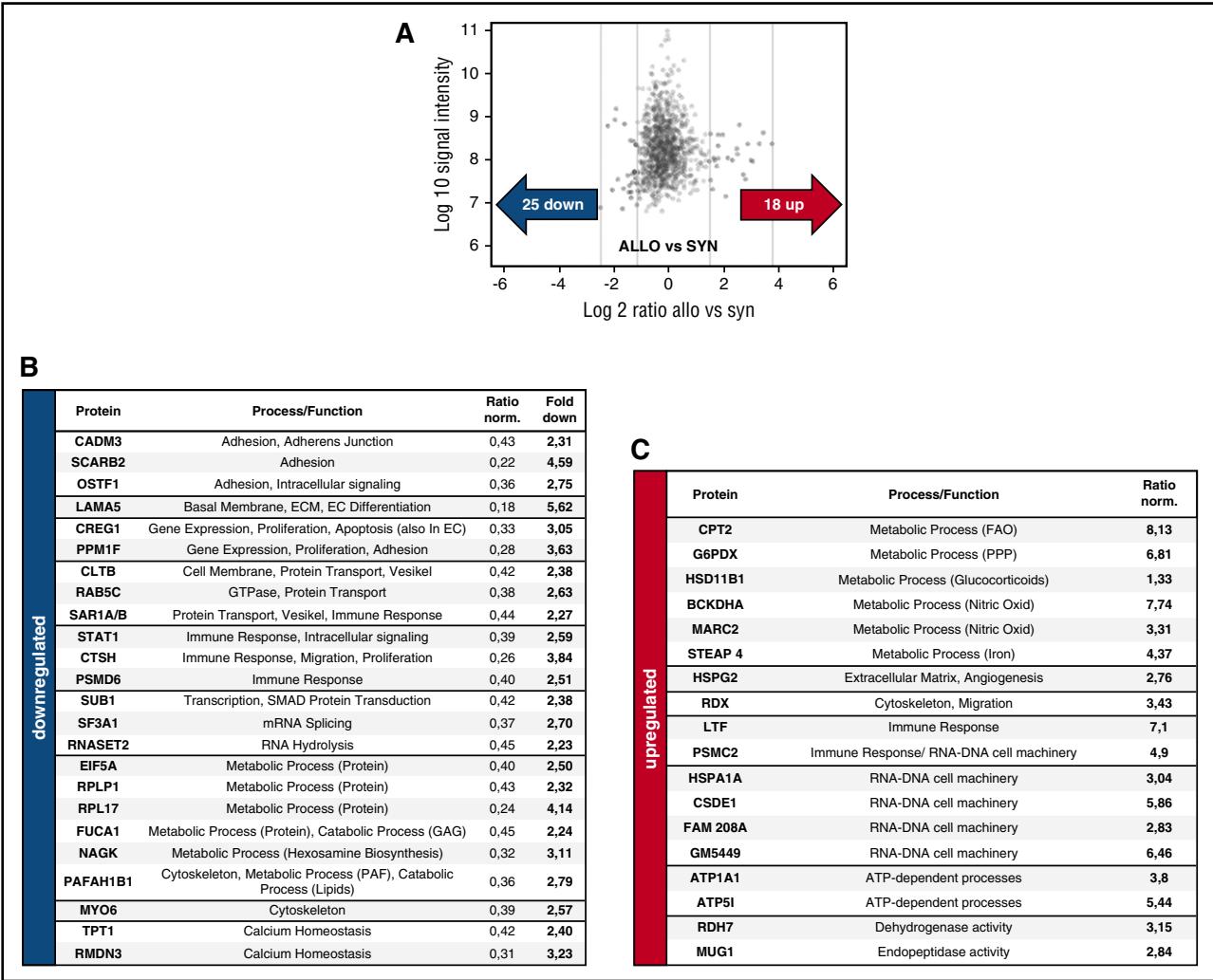
Figure 4. Microarray analysis of colon ECs reveals profound metabolic and cytoskeletal changes during initiation of angiogenesis in GVHD. (A) Hierarchical clustering of microarray data from colon ECs from ALLO and SYN mice at day+2 after BMT (LP/J→C57BL/6) (n = 4 per group). Red and blue represent high and low levels of gene expression, respectively. (B) Selected pathways with involved genes being differentially expressed in ECs between ALLO and SYN mice. In supplemental Tables 1 and 2, a detailed list of gene symbols + names, fold changes, and P values is available. (C) Volcano plot for the expression of total genes (34 472 genes). Red and blue crosses represent 145 upregulated and 99 downregulated genes, respectively. (Fold Change [linear] < −2 or >2, analysis of variance P value (Condition pair) < .05).

RNA level as well as on protein level (Figures 4B and 5B,C). In addition, we found several differentially regulated cytoskeleton-associated and -related genes (*Tubal3*, *Myo3a*, *Scin*, *Ttll6*) and proteins (RDX, MYO6) in colon and liver EC in initial GVHD (Figures 4B and 5B,C).

To investigate if metabolic and cytoskeletal changes in ECs during the initiation of GVHD have functional consequences, we measured single-cell mechanical characteristics at high speed with RT-DC[26] (Figure 6A). ECs from allo-BMT recipients and syn-BMT recipients at day+2 displayed heterogeneity in cell shape (Figure 6B). Liver ECs from allo-BMT recipients showed a significantly higher deformation ($D = 0.0547 \pm 0.0011$) as compared with ECs from syn-BMT recipients ($D = 0.0451 \pm 0.0010$) (Figure 6C-D) at day+2 after BMT. This deformation is attended by the overall softening of ECs during the initiation of GVHD. The cell size was not affected (Figure 6D). In addition to the observed downregulation of cell-cell contact proteins and the upregulation of cytoskeleton-associated proteins (described above), the EC softening indicates an enhanced migratory potential.

Discussion

It is well known that inflammatory diseases are associated with angiogenesis. The proposed mechanism for this association is an induction of angiogenesis by secreted mediators of tissue infiltrating inflammatory cells.[6,7] In this study, we provide novel evidence on a primary involvement of angiogenesis in the initiation of tissue inflammation prior to infiltration of inflammatory cells. We demonstrate that angiogenesis precedes leukocyte infiltration during inflammation in animal models of GVHD. We confirmed our finding in an experimental model of IBD, implicating a broader significance of our results surpassing the field of transplantation biology.

Our current results add further data to the accumulating evidence on the significant importance of endothelial function for the pathophysiology of GVHD. Findings from preclinical models, demonstrating that GVHD is associated with the formation of new blood vessels, were confirmed in humans.[2-5] Furthermore, endothelial pathology was specifically connected to mortality in patients with GVHD.[32,33] First mechanistic insights in therapeutic targeting angiogenesis by inhibiting the endothelial adhesion molecules VE-cadherin and α_v integrin in murine GVHD models potentially opened a new field of GVHD treatment options.[2-4] In the present study, we found that initial angiogenesis specifically arose after allo-BMT independently from syn-BMT or conditioning underlining the particular role of angiogenesis for GVHD pathogenesis.

Our results can be used as rationale for the translational development of anti-inflammatory therapies aimed at angiogenesis. With our finding that certain metabolic and cytoskeleton changes are involved in the initiation of inflammatory angiogenesis, we provide potential targets for anti-inflammatory therapies aimed at angiogenesis. Recent

A

B

Protein	Process/Function	Ratio norm.	Fold down
CADM3	Adhesion, Adherens Junction	0,43	2,31
SCARB2	Adhesion	0,22	4,59
OSTF1	Adhesion, Intracellular signaling	0,36	2,75
LAMA5	Basal Membrane, ECM, EC Differentiation	0,18	5,62
CREG1	Gene Expression, Proliferation, Apoptosis (also In EC)	0,33	3,05
PPM1F	Gene Expression, Proliferation, Adhesion	0,28	3,63
CLTB	Cell Membrane, Protein Transport, Vesikel	0,42	2,38
RAB5C	GTPase, Protein Transport	0,38	2,63
SAR1A/B	Protein Transport, Vesikel, Immune Response	0,44	2,27
STAT1	Immune Response, Intracellular signaling	0,39	2,59
CTSH	Immune Response, Migration, Proliferation	0,26	3,84
PSMD6	Immune Response	0,40	2,51
SUB1	Transcription, SMAD Protein Transduction	0,42	2,38
SF3A1	mRNA Splicing	0,37	2,70
RNASET2	RNA Hydrolysis	0,45	2,23
EIF5A	Metabolic Process (Protein)	0,40	2,50
RPLP1	Metabolic Process (Protein)	0,43	2,32
RPL17	Metabolic Process (Protein)	0,24	4,14
FUCA1	Metabolic Process (Protein), Catabolic Process (GAG)	0,45	2,24
NAGK	Metabolic Process (Hexosamine Biosynthesis)	0,32	3,11
PAFAH1B1	Cytoskeleton, Metabolic Process (PAF), Catabolic Process (Lipids)	0,36	2,79
MYO6	Cytoskeleton	0,39	2,57
TPT1	Calcium Homeostasis	0,42	2,40
RMDN3	Calcium Homeostasis	0,31	3,23

downregulated

C

| Protein	Process/Function	Ratio norm.
CPT2	Metabolic Process (FAO)	8,13
G6PDX	Metabolic Process (PPP)	6,81
HSD11B1	Metabolic Process (Glucocorticoids)	1,33
BCKDHA	Metabolic Process (Nitric Oxid)	7,74
MARC2	Metabolic Process (Nitric Oxid)	3,31
STEAP 4	Metabolic Process (Iron)	4,37
HSPG2	Extracellular Matrix, Angiogenesis	2,76
RDX	Cytoskeleton, Migration	3,43
LTF	Immune Response	7,1
PSMC2	Immune Response/ RNA-DNA cell machinery	4,9
HSPA1A	RNA-DNA cell machinery	3,04
CSDE1	RNA-DNA cell machinery	5,86
FAM 208A	RNA-DNA cell machinery	2,83
GM5449	RNA-DNA cell machinery	6,46
ATP1A1	ATP-dependent processes	3,8
ATP5I	ATP-dependent processes	5,44
RDH7	Dehydrogenase activity	3,15
MUG1	Endopeptidase activity	2,84

upregulated

Figure 5. LC-MS/MS proteome analysis of liver ECs reveals profound metabolic and cytoskeletal changes during initiation of angiogenesis in GVHD. (A) LC-MS/MS proteome analysis of liver ECs at day+2 after BMT (LP/J→C57BL/6) with 1518 proteins, and >24 000 peptides quantified revealed 25 proteins downregulated and 18 upregulated proteins between ALLO and SYN mice (n = 5 per group). (B-C) Table of downregulated and upregulated proteins with corresponding functions/mechanisms and normalized ratios. In supplemental Tables 3 and 4, a detailed list of protein symbols + names, cellular localization, and involved pathways is available. ATP, adenosine triphosphate; GAG, glycosaminoglycans; PAF, platelet activating factor; PPP, pentose phosphate pathway.

research has demonstrated that metabolic processes are linked to increased proliferative activity and vessel sprouting.[11-15,17,34-36] Inhibition of glycolysis by the 6-phosphofructo-2-kinase/fructose-2,6-biphosphatase inhibitor 3-(3-pyridinyl)-1-(4-pyridinyl)-2-propen-1-one (3PO)[17,37] as well as inhibition of FAO by etomoxir[15] showed beneficial antiangiogenic effects in several inflammatory models. Interestingly, FAO inhibitors such as ranolazine or perhexiline are clinically available and showed good drug tolerability in humans.[38] Glycolysis has been shown to be associated with remodeling of the cytoskeleton during EC migration and angiogenesis.[16,36] Accordingly, we found several differentially regulated cytoskeleton-associated and cytoskeleton-related genes and proteins in colon and liver EC in initial GVHD. Cell shape alterations by the cytoskeleton were shown to be critical for various steps of angiogenesis.[39] Cytoskeletal remodeling–dependent elevated proliferation was previously shown to soften cells in vitro.[25,40] We used a novel method, termed RT-DC,[26] to demonstrate that cytoskeleton changes result in higher deformability of ECs during the initiation of inflammation leading to increased proliferation and migration potential. The endothelial cytoskeleton can be efficiently targeted by microtubule depolymerizing agents belonging to the large group of small molecular weight vascular disrupting agents. Several of them, including the lead compound disodium combretastatin A-4 3-O-phosphate, are currently under clinical development for cancer.[41-44] In addition, there are new approaches to directly target ECs, eg, by a multimodular recombinant protein, E-selectin-specific "sneaking ligand construct" 1 (SLC1), which only binds to cytokine-activated ECs, providing the opportunity to minimize toxicity and off-target effects.[45] However, before translating our results into the clinical setting, functional analyses of pathways and therapeutic targets in preclinical models are needed. In addition, it has to be considered that the endothelium is damaged during conditioning therapy and during later phases of GVHD. Possible unwanted effects of antiangiogenic therapy on endothelial regeneration in these settings have to be addressed prior to translation of such therapeutic approaches.

The optimal schedule of an antiangiogenic treatment in inflammatory diseases represents a challenging question.[9] We showed that angiogenesis occurred as early as day+2 after BMT. Our data are in line with previous observations demonstrating that angiogenesis can be a dynamic and fast process during trauma, inflammation, and cancer
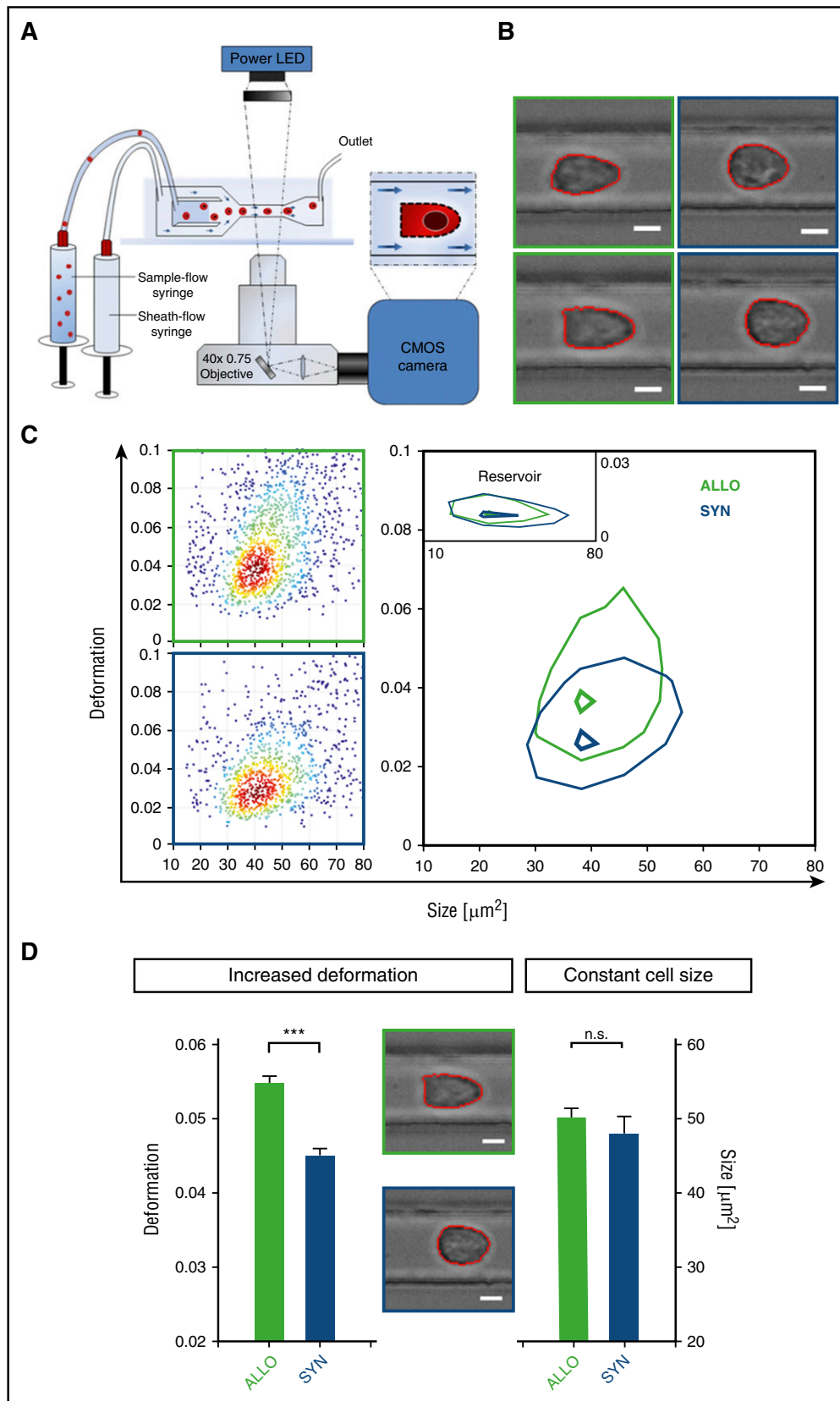
Figure 6. Early modifications in ECs have significant functional consequences as indicated by profoundly higher deformation in RT-DC. (A) RT-DC setup and measurement principle (inset shows top view of constriction). (B) Representative images of liver ECs from ALLO (green square) and SYN (blue square) mice at day+2 after BMT (LP/J→C57BL/6) acquired by RT-DC. (C) RT-DC measurements. Scatter plot of deformation vs cell size (cross-sectional area) of 1510 cells (dots). Color indicates a linear density scale. Density contour plots (50%) of ALLO vs SYN mice. (D) Mechanical phenotyping of liver ECs of ALLO and SYN mice at day+2 after BMT (LP/J→C57BL/6). Mean values n = 3. Deformation P = .0002, size P = .285 (***P ≤ .001) by a likelihood ratio test. Images are analyzed for cell size and cell shape (red contours). Scale bar, 5 μm. CMOS, complementary metal-oxide-semiconductor; LED, light-emitting diode.

growth.[46,47] Under conditions requiring rapid angiogenesis, such as wound healing, the microenvironment is quickly shifted, enabling development of new vessels within days.[48,49] As immune cell infiltration is known to contribute to resistance against antiangiogenic drugs,[50,51] starting a therapy prior to that could diminish these mechanisms as well as inflammatory-associated side effects. In the setting of GVHD, it offers the opportunity to initiate treatment early and potentially prevent or initially minimize disease outbreak.

Our current data argue against an important role of the *Vegfa/VEGFR-1/2* pathway for GVHD pathophysiology. The role and dynamics of VEGF differ in human GVHD; whereas several studies showed no change[52] or even decreased[53-55] circulating VEGFA levels, Medinger et al[5] detected an increase in VEGF$^+$ megakaryocytes going in line with increased VEGF levels found by Porkholm et al[56] in pediatric GVHD patients. However, this study only applied a univariate analysis. In a univariate and multivariate study by Luft et al, VEGF levels were not found to be predictive in GVHD; only during refractory GVHD were angiopoetin2/VEGFA ratios higher.[57] Detected differences in VEGF levels may occur due to different posttransplant time points of determination, different measurement assays, VEGF sources (eg, serum in patients vs organ biopsies in our study), or varying GVHD progression. For example, severe course of GVHD was found associated with activation and infiltration of macrophages,[58-61] which are known to be a source of VEGF.[62-64] The clinical setting in GVHD is variable due to different drug applications, particularly preexisting diseases or treatments, which modify a growth factor pathway in many ways. These findings underline the importance of identifying VEGF-independent pathways and treatment options during pathogenic angiogenesis.[29,65]

During inflammatory activation, ECs can upregulate MHC-II and also exhibit antigen-presenting properties as described in human allografts[66] and various inflammatory diseases, eg, rheumatoid arthritis.[67] In a highly inflammatory tissue environment during established GVHD, we found increased expression levels of adhesion molecules responsible for leukocyte trafficking and endothelial activation in GVHD target organs, which confirms previous knowledge.[68,69] In contrast, we found that initial endothelial activation during GVHD is not associated with upregulation of adhesion molecules and MHC-II, which is in line with results from patient biopsies during early GVHD.[70,71] A similar EC phenotype with reduced expression of adhesion molecules has been demonstrated in malignant tumors during pathological angiogenesis.[72-74] Our data demonstrate that early angiogenesis during the initiation of inflammation differs from the EC activation pattern, which is found during established tissue inflammation.

In conclusion, we provide novel insights into the initiation phase of inflammation and in GVHD pathophysiology. Our study adds evidence to the hypothesis that angiogenesis is involved in the initiation of tissue inflammation during inflammatory diseases. Our results strengthen the scientific rationale, and provide potential therapeutic targets, for development of antiangiogenic therapies to inhibit inflammation.

Authorship

Contribution: K.R., Y.S., J.M., and O.P. designed the study; K.R., M. Kalupa, A.M., S.M., S.C., J.M., and S.W. performed GVHD and colitis experiments; A.J., M. Kräter, and J.G. performed real-time deformability experiments; J.-F.S. performed FACS; D.P.-H. and G.D. performed MS experiments; K.R. analyzed data; and K.R., A.J., M. Kräter, C.S., and O.P. wrote the manuscript.

Conflict-of-interest disclosure: The authors declare no competing financial interests.

The current affiliation for S.W. is Department of Anesthesiology, Intensive Care and Pain Therapy, University Hospital Frankfurt, Frankfurt/Main, Germany.

The current affiliation for G.D. is Proteome and Genome Research Unit, Luxembourg Institute of Health, Strassen, Luxembourg.

Correspondence: Katarina Riesner, Department of Hematology, Oncology and Tumor Immunology, Charité University Medicine Berlin, Augustenburger Platz 1, 13353 Berlin, Germany; e-mail: katarina.riesner@charite.de.

References

1. Tichelli A, Gratwohl A. Vascular endothelium as 'novel' target of graft-versus-host disease. *Best Pract Res Clin Haematol*. 2008;21(2):139-148.

2. Penack O, Socié G, van den Brink MR. The importance of neovascularization and its inhibition for allogeneic hematopoietic stem cell transplantation. *Blood*. 2011;117(16):4181-4189.

3. Leonhardt F, Grundmann S, Behe M, et al. Inflammatory neovascularization during graft-versus-host disease is regulated by αv integrin and miR-100. *Blood*. 2013;121(17):3307-3318.

4. Penack O, Henke E, Suh D, et al. Inhibition of neovascularization to simultaneously ameliorate graft-vs-host disease and decrease tumor growth. *J Natl Cancer Inst*. 2010;102(12):894-908.

5. Medinger M, Tichelli A, Bucher C, et al. GVHD after allogeneic haematopoietic SCT for AML: angiogenesis, vascular endothelial growth factor and VEGF receptor expression in the BM. *Bone Marrow Transplant*. 2013;48(5):715-721.

6. Szade A, Grochot-Przeczek A, Florczyk U, Jozkowicz A, Dulak J. Cellular and molecular mechanisms of inflammation-induced angiogenesis. *IUBMB Life*. 2015;67(3):145-159.

7. Szekanecz Z, Koch AE. Mechanisms of Disease: angiogenesis in inflammatory diseases. *Nat Clin Pract Rheumatol*. 2007;3(11):635-643.

8. Tas SW, Maracle CX, Balogh E, Szekanecz Z. Targeting of proangiogenic signalling pathways in chronic inflammation. *Nat Rev Rheumatol*. 2016;12(2):111-122.

9. Welti J, Loges S, Dimmeler S, Carmeliet P. Recent molecular discoveries in angiogenesis and antiangiogenic therapies in cancer. *J Clin Invest*. 2013;123(8):3190-3200.

10. Eltzschig HK, Carmeliet P. Hypoxia and inflammation. *N Engl J Med*. 2011;364(7):656-665.

11. Cantelmo AR, Brajic A, Carmeliet P. Endothelial metabolism driving angiogenesis: emerging concepts and principles. *Cancer J*. 2015;21(4):244-249.

12. Eelen G, de Zeeuw P, Simons M, Carmeliet P. Endothelial cell metabolism in normal and diseased vasculature. *Circ Res*. 2015;116(7):1231-1244.

13. Vandekeere S, Dewerchin M, Carmeliet P. Angiogenesis revisited: an overlooked role of endothelial cell metabolism in vessel sprouting. *Microcirculation*. 2015;22(7):509-517.

14. Harjes U, Kalucka J, Carmeliet P. Targeting fatty acid metabolism in cancer and endothelial cells. *Crit Rev Oncol Hematol*. 2016;97:15-21.

15. Schoors S, Bruning U, Missiaen R, et al. Fatty acid carbon is essential for dNTP synthesis in endothelial cells. *Nature*. 2015;520(7546): 192-197.

16. De Bock K, Georgiadou M, Schoors S, et al. Role of PFKFB3-driven glycolysis in vessel sprouting. *Cell*. 2013;154(3):651-663.

17. Schoors S, De Bock K, Cantelmo AR, et al. Partial and transient reduction of glycolysis by PFKFB3 blockade reduces pathological angiogenesis. *Cell Metab*. 2014;19(1):37-48.

18. Chidlow JH Jr, Shukla D, Grisham MB, Kevil CG. Pathogenic angiogenesis in IBD and experimental colitis: new ideas and therapeutic avenues. *Am J Physiol Gastrointest Liver Physiol*. 2007;293(1): G5-G18.

19. Danese S, Sans M, Spencer DM, et al. Angiogenesis blockade as a new therapeutic approach to experimental colitis. *Gut*. 2007;56(6): 855-862.

20. Costa C, Incio J, Soares R. Angiogenesis and chronic inflammation: cause or consequence? *Angiogenesis*. 2007;10(3):149-166.

21. Boersema PJ, Raijmakers R, Lemeer S, Mohammed S, Heck AJ. Multiplex peptide stable isotope dimethyl labeling for quantitative proteomics. *Nat Protoc*. 2009;4(4):484-494.

22. Rappsilber J, Mann M, Ishihama Y. Protocol for micro-purification, enrichment, pre-fractionation and storage of peptides for proteomics using StageTips. *Nat Protoc*. 2007; 2(8):1896-1906.

23. Cox J, Mann M. MaxQuant enables high peptide identification rates, individualized p.p.b.-range mass accuracies and proteome-wide protein quantification. *Nat Biotechnol*. 2008;26(12): 1367-1372.

24. Elias JE, Gygi SP. Target-decoy search strategy for increased confidence in large-scale protein identifications by mass spectrometry. *Nat Methods*. 2007;4(3):207-214.

25. Chan CJ, Ekpenyong AE, Golfier S, et al. Myosin II activity softens cells in suspension. *Biophys J*. 2015;108(8):1856-1869.

26. Otto O, Rosendahl P, Mietke A, et al. Real-time deformability cytometry: on-the-fly cell mechanical phenotyping. *Nat Methods*. 2015; 12(3):199-202.

27. Riesner K, Kalupa M, Shi Y, Elezkurtaj S, Penack O. A preclinical acute GVHD mouse model based on chemotherapy conditioning and MHC-matched transplantation. *Bone Marrow Transplant*. 2016; 51(3):410-417.

28. Hudlicka O, Brown M, Egginton S. Angiogenesis in skeletal and cardiac muscle. *Physiol Rev*. 1992; 72(2):369-417.

29. Ferrara N. Pathways mediating VEGF-independent tumor angiogenesis. *Cytokine Growth Factor Rev*. 2010;21(1):21-26.

30. Steinhoff G, Wonigeit K, Pichlmayr R. Analysis of sequential changes in major histocompatibility complex expression in human liver grafts after transplantation. *Transplantation*. 1988;45(2): 394-401.

31. Marelli-Berg FM, Jarmin SJ. Antigen presentation by the endothelium: a green light for antigen-specific T cell trafficking? *Immunol Lett*. 2004; 93(2-3):109-113.

32. Dietrich S, Falk CS, Benner A, et al. Endothelial vulnerability and endothelial damage are associated with risk of graft-versus-host disease and response to steroid treatment. *Biol Blood Marrow Transplant*. 2013;19(1):22-27.

33. Rachakonda SP, Penack O, Dietrich S, et al. Single-nucleotide polymorphisms within the thrombomodulin gene (THBD) predict mortality in patients with graft-versus-host disease. *J Clin Oncol*. 2014;32(30):3421-3427.

34. Schoors S, Bruning U, Missiaen R, et al. Corrigendum: fatty acid carbon is essential for dNTP synthesis in endothelial cells. *Nature*. 2015; 526(7571):144.

35. Takuwa Y, Du W, Qi X, Okamoto Y, Takuwa N, Yoshioka K. Roles of sphingosine-1-phosphate signaling in angiogenesis. *World J Biol Chem*. 2010;1(10):298-306.

36. Uebelhoer M, Iruela-Arispe ML. Cross-talk between signaling and metabolism in the vasculature. *Vascul Pharmacol*. 2016;83:4-9.

37. Xu Y, An X, Guo X, et al. Endothelial PFKFB3 plays a critical role in angiogenesis. *Arterioscler Thromb Vasc Biol*. 2014;34(6):1231-1239.

38. Carracedo A, Cantley LC, Pandolfi PP. Cancer metabolism: fatty acid oxidation in the limelight. *Nat Rev Cancer*. 2013;13(4):227-232.

39. Bayless KJ, Johnson GA. Role of the cytoskeleton in formation and maintenance of angiogenic sprouts. *J Vasc Res*. 2011;48(5):369-385.

40. Lautenschläger F, Paschke S, Schinkinger S, Bruel A, Beil M, Guck J. The regulatory role of cell mechanics for migration of differentiating myeloid cells. *Proc Natl Acad Sci USA*. 2009;106(37): 15696-15701.

41. Kanthou C, Tozer GM. The tumor vascular targeting agent combretastatin A-4-phosphate induces reorganization of the actin cytoskeleton and early membrane blebbing in human endothelial cells. *Blood*. 2002;99(6):2060-2069.

42. Kanthou C, Tozer GM. Microtubule depolymerizing vascular disrupting agents: novel therapeutic agents for oncology and other pathologies. *Int J Exp Pathol*. 2009;90(3): 284-294.

43. Kim S, Peshkin L, Mitchison TJ. Vascular disrupting agent drug classes differ in effects on the cytoskeleton. *PLoS One*. 2012;7(7):e40177.

44. Shi Y, Zhang L, Pu H, et al. Rapid endothelial cytoskeletal reorganization enables early blood-brain barrier disruption and long-term ischaemic reperfusion brain injury. *Nat Commun*. 2016;7: 10523.

45. Sehnert B, Burkhardt H, Wessels JT, et al. NF-κB inhibitor targeted to activated endothelium demonstrates a critical role of endothelial NF-κB in immune-mediated diseases. *Proc Natl Acad Sci USA*. 2013;110(41):16556-16561.

46. Roudier E, Gineste C, Wazna A, Dehghan K, Desplanches D, Birot O. Angio-adaptation in unloaded skeletal muscle: new insights into an early and muscle type-specific dynamic process. *J Physiol*. 2010;588(Pt 22):4579-4591.

47. Kreuger J, Phillipson M. Targeting vascular and leukocyte communication in angiogenesis, inflammation and fibrosis. *Nat Rev Drug Discov*. 2016;15(2):125-142.

48. Leibovich SJ, Wiseman DM. Macrophages, wound repair and angiogenesis. *Prog Clin Biol Res*. 1988;266:131-145.

49. De Raeve H, Van Marck E, Van Camp B, Vanderkerken K. Angiogenesis and the role of bone marrow endothelial cells in haematological malignancies. *Histol Histopathol*. 2004;19(3): 935-950.

50. Shojaei F. Anti-angiogenesis therapy in cancer: current challenges and future perspectives. *Cancer Lett*. 2012;320(2):130-137.

51. Shojaei F, Wu X, Malik AK, et al. Tumor refractoriness to anti-VEGF treatment is mediated by CD11b+Gr1+ myeloid cells. *Nat Biotechnol*. 2007;25(8):911-920.

52. Moiseev IS, Lapin SV, Surkova EA, Lerner MY, Vavilov VN, Afanasyev BV. Level of vascular endothelial growth factor predicts both relapse and nonrelapse mortality after allogeneic hematopoietic stem cell transplantation. *Biol Blood Marrow Transplant*. 2013;19(12): 1677-1682.

53. Holtan SG, Verneris MR, Schultz KR, et al. Circulating angiogenic factors associated with response and survival in patients with acute graft-versus-host disease: results from Blood and Marrow Transplant Clinical Trials Network 0302 and 0802. *Biol Blood Marrow Transplant*. 2015; 21(6):1029-1036.

54. Min CK, Kim SY, Lee MJ, et al. Vascular endothelial growth factor (VEGF) is associated with reduced severity of acute graft-versus-host disease and nonrelapse mortality after allogeneic stem cell transplantation. *Bone Marrow Transplant*. 2006;38(2):149-156.

55. Nachbaur D, Schumacher P, Auberger J, Clausen J, Kircher B. Vascular endothelial growth factor and activin-a serum levels following allogeneic hematopoietic stem cell transplantation. *Biol Blood Marrow Transplant*. 2007;13(8):942-947.

56. Porkholm M, Bono P, Saarinen-Pihkala UM, Kivivuori SM. Higher angiopoietin-2 and VEGF levels predict shorter EFS and increased non-relapse mortality after pediatric hematopoietic SCT. *Bone Marrow Transplant*. 2013;48(1):50-55.

57. Luft T, Dietrich S, Falk C, et al. Steroid-refractory GVHD: T-cell attack within a vulnerable endothelial system. *Blood*. 2011;118(6): 1685-1692.

58. Hülsdünker J, Zeiser R. Insights into the pathogenesis of GvHD: what mice can teach us about man. *Tissue Antigens*. 2015;85(1):2-9.

59. Alexander KA, Flynn R, Lineburg KE, et al. CSF-1-dependant donor-derived macrophages mediate chronic graft-versus-host disease. *J Clin Invest*. 2014;124(10):4266-4280.

60. Terakura S, Martin PJ, Shulman HM, Storer BE. Cutaneous macrophage infiltration in acute GvHD. *Bone Marrow Transplant*. 2015;50(8): 1135-1137.

61. Nogai A, Shi Y, Pérez-Hernandez D, et al. Organ siderosis and hemophagocytosis during acute graft-versus-host disease. *Haematologica*. 2016; 101(8):e344-e346.

62. Ramanathan M, Pinhal-Enfield G, Hao I, Leibovich SJ. Synergistic up-regulation of vascular endothelial growth factor (VEGF) expression in macrophages by adenosine A2A receptor agonists and endotoxin involves transcriptional regulation via the hypoxia response element in the VEGF promoter. *Mol Biol Cell*. 2007;18(1):14-23.

63. Crowther M, Brown NJ, Bishop ET, Lewis CE. Microenvironmental influence on macrophage regulation of angiogenesis in wounds and malignant tumors. *J Leukoc Biol*. 2001;70(4): 478-490.

64. Ferrara N, Davis-Smyth T. The biology of vascular endothelial growth factor. *Endocr Rev*. 1997; 18(1):4-25.

65. Sengupta S, Gherardi E, Sellers LA, Wood JM, Sasisekharan R, Fan TP. Hepatocyte growth factor/scatter factor can induce angiogenesis independently of vascular endothelial growth factor. *Arterioscler Thromb Vasc Biol*. 2003;23(1): 69-75.

66. Turesson C. Endothelial expression of MHC class II molecules in autoimmune disease. *Curr Pharm Des*. 2004;10(2):129-143.

67. Mai J, Virtue A, Shen J, Wang H, Yang XF. An evolving new paradigm: endothelial cells–conditional innate immune cells. *J Hematol Oncol*. 2013;6:61.

68. Eyrich M, Burger G, Marquardt K, et al. Sequential expression of adhesion and costimulatory molecules in graft-versus-host disease target organs after murine bone marrow transplantation across minor histocompatibility antigen barriers.

Biol Blood Marrow Transplant. 2005;11(5): 371-382.

69. Lu SX, Holland AM, Na IK, et al. Absence of P-selectin in recipients of allogeneic bone marrow transplantation ameliorates experimental graft-versus-host disease. *J Immunol.* 2010; 185(3):1912-1919.

70. Norton J, al-Saffar N, Sloane JP. Adhesion molecule expression in human hepatic graft-versus-host disease. *Bone Marrow Transplant.* 1992;10(2):153-156.

71. Norton J, Sloane JP, Delia D, Greaves MF. Reciprocal expression of CD34 and cell adhesion molecule ELAM-1 on vascular endothelium in acute cutaneous graft-versus-host disease. *J Pathol.* 1993;170(2):173-177.

72. Dirkx AE, oude Egbrink MG, Castermans K, et al. Anti-angiogenesis therapy can overcome endothelial cell anergy and promote leukocyte-endothelium interactions and infiltration in tumors. *FASEB J.* 2006;20(6):621-630.

73. Griffioen AW, Damen CA, Blijham GH, Groenewegen G. Tumor angiogenesis is accompanied by a decreased inflammatory response of tumor-associated endothelium. *Blood.* 1996;88(2):667-673.

74. Dirkx AE, Oude Egbrink MG, Kuijpers MJ, et al. Tumor angiogenesis modulates leukocyte-vessel wall interactions in vivo by reducing endothelial adhesion molecule expression. *Cancer Res.* 2003;63(9):2322-2329.